

Covering the Fermi Surface with Patches of Quarkyonic Chiral Spirals

Toru Kojo^a, Robert D. Pisarski^b, and A. M. Tsvelik^c

^a*RIKEN/BNL Research Center,
Brookhaven National Laboratory Upton,
NY-11973, USA*

^b*Department of Physics,
Brookhaven National Laboratory Upton,
NY-11973, USA*

^c*Department of Physics,
Department of Condensed Matter Physics and Materials Science,
Brookhaven National Laboratory,
Upton, NY 11973-5000, USA*

(Dated: October 26, 2018)

Abstract

We argue that in cold, dense quark matter, in the limit of a large number of colors the ground state is unstable with respect to creation of a complicated Quarkyonic Chiral Spiral (QCS) state, in which both chiral and translational symmetries are spontaneously broken. The entire Fermi surface is covered with patches of QCSs, whose number increases as the quark density does. The low energy excitations are gapless, given by Wess-Zumino-Novikov-Witten model plus transverse kinetic terms localized about different patches.

PACS numbers:

Keywords:

I. INTRODUCTION

In cold, dense quark matter, one expects several phenomenon: a transition to a deconfined phase, color superconductivity [1], and for a large number of colors, N_c , chiral density waves [2–5].

Recent theoretical work has argued that at least for a large number of colors, N_c , further phenomena can occur [6–12]. There can be a phase in which the baryon density is large, but that is nevertheless confining. While such a “Quarkyonic” phase is certainly present at large N_c , it also exhibits several properties which may have been observed in experiments at the CERN SPS [9].

Ref. [10] suggests that in a Quarkyonic phase, the *local* breaking of chiral symmetry is driven by the appearance of chiral density waves, which were termed Quarkyonic Chiral Spirals (QCS). This arises from the condensation of particle-hole pairs near the Fermi surface, and is similar to the mechanism of chiral condensation in the vacuum. The essential difference is that in the presence of a Fermi sea, the dominant condensation involves a particle-hole pairs with nearly opposite Fermi momentum. The net momentum of the pair is then nonzero and large, so that not only chiral symmetry, but also translational symmetry, is spontaneously broken through the formation of a chiral condensate which was termed a (Quarkyonic) Chiral Spiral. This condensate rotates between the usual chiral condensate, $\bar{\psi}\psi$, and a helicity condensate, $\bar{\psi}\gamma_0\gamma_z\psi$. This is closely analogous to a chiral spiral in 1 + 1 dimensions, which rotates between $\bar{\psi}\psi$ and $\bar{\psi}\gamma_5\psi$ [13].

The analysis in Ref. [10] was restricted to chiral spirals which form in one direction. In this paper we argue that the entire Fermi surface is covered with patches of QCSs, where each patch corresponds to a different direction for a single QCS. The long-range forces present in Quarkyonic matter imply that the gaps are strongly momentum dependent. As a consequence, at large angles the interaction between particles and QCSs is suppressed, and QCSs at large angles to one another interact weakly.

We estimate the width of the patches, and find that the number of patches increases with the density. As the density increases, the Fermi surface is characterized by increasingly high symmetry, and a series of phase transitions occur. All of these transitions occur in a confined phase with locally broken chiral symmetry, and thus are distinct from the transitions for the restoration of chiral symmetry, or for deconfinement.

Ref. [10] showed that QCSs dominate at intermediate chemical potentials, up to $\mu \sim 80$ GeV. At higher μ , the effects of perturbative interactions must also be included, and also generate chiral spirals. It was previously suggested in Refs. [3] and [4] that perturbative chiral spirals also cover the Fermi sphere in patches. Our analysis extends and compliments theirs.

II. THE QUALITATIVE PICTURE FOR THE CONFINING MODEL

In the limit of large N_c , the gluon propagator is unaffected by the quarks. This means that at low temperature, the gluon propagator is the same as in the confined vacuum. We thus use the effective gluon propagator

$$D_{00}(\omega, \mathbf{q}) = \frac{\sigma}{|\mathbf{q}^2|^2}, \quad D_{ik}(\omega, \mathbf{q}) = \frac{\delta_{ik} - q_i q_k / q^2}{\omega^2 + \mathbf{q}^2}. \quad (1)$$

This propagator is valid in Coulomb gauge, $\partial_i A_i = 0$, at small momenta, $|\mathbf{q}| < \Lambda_{\text{QCD}}$. This propagator is very long range, and through the exchange of A_0 fields, strongly enhances the density-density interaction at small momentum transfer. This reflects the linear confinement of mesonic excitations. Following [10], we concentrate on nonperturbative contributions from D_{00} and ignore perturbative effects from D_{ik} .

We summarize the results of [10], and give a qualitative interpretation which we use to construct a Fermi surface with multiple patches. Taking the gluon propagator D_{00} of Eq. (1), the Schwinger-Dyson equation for the quark self energy can be constructed, especially for excitations near the Fermi surface. It is

$$\Sigma(p) + \Sigma_m(p) = - \int \frac{d^4 k}{(2\pi)^4} (\gamma_0 t_A) S(k; \Sigma) (\gamma_0 t_B) D_{00}^{AB}(p - k). \quad (2)$$

Near the Fermi surface, $p_z \sim \mu$, and $|\mathbf{p}_T| \sim 0$. Since the dominant contributions come from interactions with small momentum transfer, the integral is dominated by virtual quarks within $\sim \Lambda_{\text{QCD}}$ of the edge of the Fermi sea. In this region the transverse momenta of the quarks can be ignored, and the integral equation factorizes,

$$\int dk_0 dk_z d^2 \mathbf{k}_T S(k_0, k_z, \mathbf{k}_T) D_{00}(p - k) \rightarrow \int dk_0 dk_z S(k_0, k_z, \mathbf{0}_T) \int d\mathbf{k}_T D_{00}(p - k). \quad (3)$$

Integrating over the gluon propagator over \mathbf{k}_T gives the Schwinger-Dyson equation for QCD in 1 + 1 dimensions in axial gauge, $A_z = 0$.

When spatial dimensions are compactified, usually motion in the small, compact dimensions is energetically disfavored. In contrast, here the quarks move easily in the transverse dimension, with essentially no energetic penalty. Thus counting the number of states with different transverse momenta matters, and is taken into account in the second integral of Eq. (3). This smears the four dimensional, confining gluon propagators, and reduces them to propagators in two dimensions.

Next consider the particle-hole correlations. These can be treated in a Bethe-Salpeter equation for quarks and quark holes, matching north and south poles of the Fermi sea. By the same reasoning as applies for the Schwinger-Dyson equation, the Bethe-Salpeter equation also reduces to that for QCD in two dimensions.

One might ask why we only choose states at opposite ends of the Fermi sea, and do not simultaneously take into account contributions from the entire Fermi surface. For example, in the usual analysis of (s-wave) BCS superconductivity, the Coulomb force is additive, and one electron feels a sum of interactions from all electrons over the entire Fermi surface.

This is not true in a Quarkyonic phase. For a system with quark and quark-holes, because of confinement what is dominant is the formation of mesons between quarks and quark holes. The resulting mesonic states then interact weakly, via residual meson-meson interactions $\sim 1/N_c$. Therefore it is reasonable to first identify the most tightly bound pairs, treating interactions between the mesons as a small perturbation.

This is why we first consider a problem with two patches, and then extend this analysis to multiple patches. The most relevant pairing for two patches is the density wave channel in which quarks and quark holes move in the same direction with total momentum, $\sim 2\mu$, while keeping their relative momentum to $\sim \Lambda_{\text{QCD}}$ [10]. Confinement then drives a gap $\sim \Lambda_{\text{QCD}}$, and is not very sensitive to the quark density. This will allow us to easily estimate the transverse size of the patches.

Finally we briefly mention the mapping between quark bilinears in $3 + 1$ dimensions to those in $1 + 1$ dimensions. The basic point is that the transverse momenta is negligible relative to $\sim \mu$, so that quantities which couple to transverse momenta are subleading. Thus γ_T can be dropped, as can terms which mix spin. The spin symmetry converts to a doubled flavor symmetry in $1 + 1$ dimensions. For a dictionary of quark bilinear operators, see [10].

III. THE SINGLE PATCH PROBLEM: QUALITATIVE ARGUMENTS

In condensed matter physics, usually density waves form because of a nesting of the Fermi surface, with particle-hole pairs near the Fermi surface connected by a common wave vector [14]. In one spatial dimension, such nesting is automatic, because the boundary of the Fermi sea are just two points. This is not true in higher dimensions. For quarks in 3+1 dimensions, the boundary of the Fermi sea is spherically symmetric, and nesting cannot occur without deforming the Fermi sphere.

To develop insight into how the chiral condensate forms, we first assume that the single particle spectrum for quarks is a well defined notion. We then apply mean field theory, and ignore all of the subtleties from confinement. In the last part of this section, we argue more carefully, albeit qualitatively, as to why this might be correct.

We first consider an order parameter with only one Fourier component. We use a mean field approximation where the chiral spiral acts on quarks like a periodic background, $\sim \Delta_Q \cos(\mathbf{Q} \cdot \mathbf{r})$. This problem is mathematically equivalent to that of noninteracting electrons propagating in a crystalline periodic potential. The dispersion relations for the particle and hole branches are given by

$$E_{\pm} = \frac{\epsilon(\mathbf{p}) + \epsilon(\mathbf{p} + \mathbf{Q})}{2} \pm \sqrt{\frac{\epsilon(\mathbf{p}) - \epsilon(\mathbf{p} + \mathbf{Q})^2}{4} + |\Delta_Q|^2} \quad (4)$$

where $\epsilon(\mathbf{p})$ is the quark energy. Δ_Q is the magnitude of the condensate induced by the chiral spiral waves at a momentum \mathbf{Q} , and is treated as a variational parameter. An optimum $|\mathbf{Q}|$ should be about $2p_F$, so we can safely replace Δ_Q with $M \equiv \Delta_{2p_F}$.

Let us establish what the requirements are for \mathbf{Q} and the patch size. The z -axis is taken to penetrate a center of two patches connected by \mathbf{Q} , and the momenta \mathbf{p} is measured from $p_F \mathbf{e}_z$. Expanding the energies about the Fermi surface, and taking $Q \sim 2p_F$, $p_z \sim p_F$,

$$\begin{aligned} \epsilon(\mathbf{p}) &= \sqrt{(p_z + p_F)^2 + p_{\perp}^2} - p_F \approx p_z + \frac{p_{\perp}^2}{2p_F} + \dots, \\ \epsilon(\mathbf{p} + \mathbf{Q}) &= \sqrt{(Q - p_z - p_F)^2 + p_{\perp}^2} - p_F \approx Q - 2p_F - p_z + \frac{p_{\perp}^2}{2p_F} + \dots \end{aligned} \quad (5)$$

Substituting this into (4) gives

$$E_{\pm} \approx \frac{Q}{2} - p_F + \frac{p_{\perp}^2}{2p_F} \pm \sqrt{\left(\frac{Q}{2} - p_F - p_z\right)^2 + M^2}. \quad (6)$$

The dispersion relation for a single quark can be used to estimate the size of the patches. Energetically, the system benefits from opening as large a gap as possible. The edge of a patch occurs when a single quark becomes gapless. This reflects the balance between the condensation energy and the kinetic energy.

Thus \mathbf{Q} , and the size of the patch, is determined as follows. A lower bound for $|\mathbf{Q}|$ arises from the condition that the positive branch has nonzero energy, $E_+ \geq 0$. The minimum value of $|\mathbf{Q}|$ occurs when $E_+ = 0$; this happens for $p_\perp = 0, p_z = Q/2 - p_F$, which satisfies

$$E_+^{\min} = \frac{Q}{2} - p_F + M \geq 0. \quad (7)$$

Thus the ordering vector is not exactly $2p_F$, but a slightly smaller value, $2(p_F - M)$. The minimum value for Q is $Q_{\min} = 2(p_F - M)$, caused by the deformation of the Fermi surface (see Fig. 1).

The transverse size of the patches is determined by the condition that the lower branch has positive energy. $E_- = 0$ occurs when

$$p_z = \frac{Q}{2} - p_F = -M, \quad \frac{(p_\perp^{\max})^2}{2p_F} = M. \quad (8)$$

For later use, we refer to $p_\perp^{\max} = \sqrt{2p_F M} = M_\perp$.

The main origin of the gap is confinement. In the Quarkyonic phase at large N_c , the string tension is independent of density, and thus so is the gap,

$$M \sim \sqrt{\sigma} \sim \Lambda_{\text{QCD}}. \quad (9)$$

Why can we use the quark dispersion relation to estimate the transverse size of the patch? After all, with a sharp infrared cutoff for the confining gluon propagator, the quark propagator has a pole which diverges as the cutoff vanishes. This divergence can be avoided with other infrared regulators, but it is worrisome.

The point is, however, that any quark excitation is inevitably accompanied by a quark hole, with the two forming a mesonic type excitation. For such wavefunctions, infrared ambiguities disappear. Consider, for example, the theory in vacuum. All quarks are confined, but it is sensible to speak of the constituent mass of a quark, approximately one half the mass of a meson. For the mesons near the Fermi surface, then, we can also speak of a constituent “mass”. The dependence of this constituent mass on the transverse momentum should be given, approximately, by our naive analysis above.

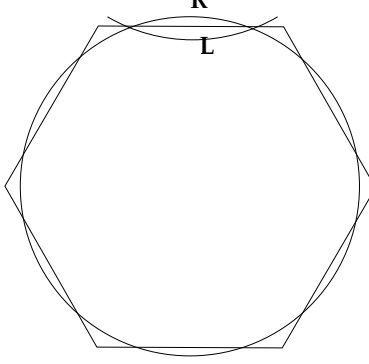


FIG. 1: The Fermi surface (FS) with three QCSs. Bringing the opposite pieces of FS demonstrates imperfect nesting. The spherical parts of the FS on each edge are approximated by Eq.(21).

Of course, the patch size can be rigorously computed by considering color singlet quantities. In $1+1$ dimensions, this can be done using non-Abelian bosonization. Detailed analysis shows that the width of the patch is $\sim p_{\perp}^{\max}$, up to a number of order one.

IV. MULTIPLE PATCHES

In the previous subsection, we considered one patch problem in $(3+1)$ dimensions. The size of the patch was estimated by computing the transverse momentum at which the gap closed. In reality, the gap remains nonzero, due to interaction with different patches. Since the size of the gap is related to that of the order parameter, different patches then interact with one another.

However, a significant simplification takes place when we take into account that the gap depends upon the virtuality of the quark. In vacuum, it is known that quarks with high virtuality, or in the deep Euclidean region, do not feel the effects of chiral symmetry breaking. This suggests that the scattering between a particle and a QCS is small if the angle between the two is large.

To see this more explicitly, note that in the presence of a QCS, the mass self-energy is

$$\sum_{i=1}^{N_p} \int \frac{d^4 p}{(2\pi)^4} \bar{\psi}(p - \mathbf{Q}_i) M(p; \mathbf{Q}_i) \psi(p) + (\text{h.c.}). \quad (10)$$

where $|\mathbf{Q}_i| \sim 2p_F$. Consider the process whereby a quark, nearly on-shell with momentum $p_0 \simeq p_F$ and $\mathbf{p} \simeq p_F \mathbf{e}_z$, scattering of a QCS with momentum \mathbf{Q}_i , and thereby acquires

momentum $\mathbf{p} - \mathbf{Q}_i$. QCSs are static, so the energy p_0 remains the same. The mass function $M(p; \mathbf{Q}_i)$ contributes if the scattered quark is on-shell within a region $\sim \Lambda_{\text{QCD}}^2$,

$$p_0^2 - (\mathbf{p} - \mathbf{Q})^2 \simeq -4p_F^2(1 - \cos\theta) \sim -\Lambda_{\text{QCD}}^2, \quad \mathbf{p} \cdot \mathbf{Q} = 2p_F^2 \cos\theta. \quad (11)$$

Thus the angle to the z -axis, θ , is limited to $|\theta| < \Lambda_{\text{QCD}}/p_F$. Physically, this is the same condition as for the collinear scattering of two quarks. This condition is special to the long range interactions in Quarkyonic matter.

Hence the mass term in (10) is dominated by patches whose angle is within 0 or π of the incident quark,

$$\sum_{i=1}^{N_p} \int \frac{d^4 p}{(2\pi)^4} \bar{\psi}(p - \mathbf{Q}_i) M(p; \mathbf{Q}_i) \psi(p) \times \theta\left(\Lambda_{\text{QCD}}^2 - |2\mathbf{p} \cdot \mathbf{Q}_i - \mathbf{Q}_i^2|\right) + (\text{h.c.}). \quad (12)$$

In the following, we will take into account interactions between nearest neighbor patches in momentum space.

From Eq.(8), the number of patches is

$$N_p \approx \frac{4p_F^2}{M_{\perp}^2} = \frac{p_F}{2M} \sim \frac{n^{1/3}}{M}, \quad (13)$$

where n is the quark density per single flavor. Thus the number of patches increases slowly with the density. Since the number of patches is an integer, it must change discontinuously. In Fig. 2 we depict a succession of four different coverings of a sphere, corresponding to different arrangements of QCSs. At the smallest density there are three mutually perpendicular QCSs, which form a cube. As the density increases, extra patches emerge at the corners of the cube, giving rise to four more QCSs, the blue shape in Fig.2. The wave vectors of the new QCSs are aligned along the diagonals of the cube, so that eight new patches emerge at the corners of the cube. Increasing the density further leads to extra patches at the corners of the blue shape, leading to the red shape, thence to the green shape, and so on.

Instead of the above construction, what if one takes smaller patches, say of size Λ_{QCD} , with a corresponding increase in the number of the patches? This is not possible, though. Because the gap arises from a confining force, the size of Q is fixed to be $|Q|/2 \sim p_F - M$. By Luttinger's theorem, the total volume of the Fermi sea is conserved, so any volume squeezed in the p_z -direction must be compensated by an extension in the transverse size, until it reaches $\sim M_{\perp}$. We expect that the presence of other patches slightly reduce the transverse

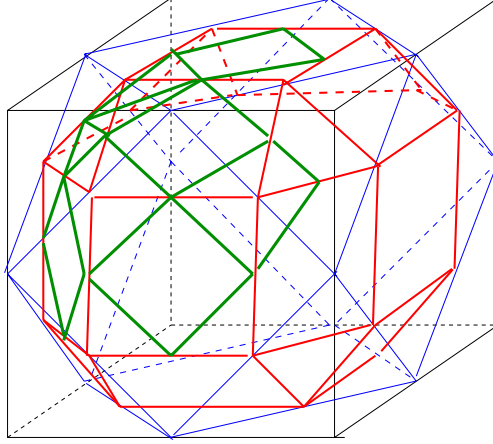


FIG. 2: A succession of QCS configurations corresponding to the different quark density. Black lines show a simple cube.

size, αM_{\perp} ($\Lambda_{\text{QCD}}/M_{\perp} \ll \alpha < 1$), while $|\mathbf{Q}|$ slightly increases from the value for one patch. Below we will determine α and $|\mathbf{Q}|$ by regarding them as variational parameters.

To match different patches onto one another, consider the part of the Fermi surface where several patches meet. From Fig. 2 it follows that the most typical configuration is where four patches meet at one corner. We want to establish the conditions for the emergence of next patch. Assuming that there are many patches, the curvature at the corners can be neglected. We also neglect the influence of all other patches except for those four which are adjacent. Then the problem reduces that of a particle subject to the potential generated by four QCSs. If $\tilde{\mathbf{Q}}$ is a vector in the direction of the corner, then the four wave vectors of the patches are $\mathbf{Q}_i = \tilde{\mathbf{Q}} \pm \alpha M_{\perp} \mathbf{e}_i$, where

$$\sum_i \mathbf{e}_i = 0, \quad \mathbf{e}_i^2 = 1, \quad \tilde{\mathbf{Q}} \cdot \mathbf{e}_i = 0, \quad M_{\perp} = \sqrt{|\tilde{\mathbf{Q}}| M} \ll |\tilde{\mathbf{Q}}|, \quad (14)$$

with $M_{\perp} = \sqrt{2p_F M}$ is the transverse size of the patches, from above. We expect that having several patches does not change this, so we take $\alpha \sim 1$. In high density, we can set $\tilde{\mathbf{Q}} \simeq \mathbf{Q}$ with $|\mathbf{Q}| = 2p_F$, and $\mathbf{Q} \cdot \mathbf{e}_i \simeq 0$.

Near the corner, the total gap is

$$\Delta_Q(\mathbf{r}) \simeq \frac{M}{4} \sum_i e^{i(\mathbf{Q} \pm \alpha M_{\perp} \mathbf{e}_i) \cdot \mathbf{r}} = \frac{M e^{i\mathbf{Q}z}}{2} \left[\cos(\alpha M_{\perp} x) + \cos(\alpha M_{\perp} y) \right]. \quad (15)$$

By the previous arguments about virtuality, only particles within $\sim \Lambda_{\text{QCD}}$ of a corner contribute. Away from the corner, where $|\mathbf{p}_{\perp}| \gg \Lambda_{\text{QCD}}$, we reduce to the previous problem of

one patch.

Since the transverse modulation occurs slowly, we can calculate the spectrum in the adiabatic approximation, separating the motion along \mathbf{Q} from the transverse motion. Initially we consider the transverse coordinates as constant parameters. Then the energy eigenstates yield the two bands of the one patch problem, Eq. (5). Next we consider the energy for the effective Hamiltonian, H_{eff}^{\pm} , describing the transverse motion of the upper (+) and lower (-) bands,

$$H_{\text{eff}}^{\pm} \simeq \left(\frac{Q}{2} - p_F \right) - \frac{1}{Q} (\nabla_{\perp})^2 \pm \sqrt{\left(k_z - \frac{Q}{2} \right)^2 + |\Delta(\mathbf{r}_{\perp})|^2},$$

$$|\Delta(\mathbf{r}_{\perp})|^2 = M^2 \left[\cos(\alpha M_{\perp} x) + \cos(\alpha M_{\perp} y) \right]^2. \quad (16)$$

This patch configuration becomes unstable when the gap between the upper and the lower bands close. This occurs first when $k_z = Q/2$. Eq. (16) is the Schrödinger equation in a periodic potential. Its solutions and eigenvalues $E_l(\mathbf{p}_{\perp})$, $l = 1, 2, \dots$, depend on the continuous variable \mathbf{p}_{\perp} (quasi-momentum) with values confined to the Brillouin zone $-\alpha M_{\perp}/2 < (p_{\perp}^x, p_{\perp}^y) < \alpha M_{\perp}/2$. The solutions are arranged so that $E_1 < E_2 < E_3 < \dots$. The given QCS configuration becomes unstable if the lowest band, $l = 1$, crosses from negative to positive energy at some value of quasi-momentum.

Taking into account (14) and making the substitution $\mathbf{r}_{\perp} \rightarrow (\alpha M_{\perp})^{-1} \mathbf{r}_{\perp}$, we get the Schrödinger equation for the transverse motion:

$$\left(-\alpha^2 (\partial_x^2 + \partial_y^2) \pm \frac{|\cos x + \cos y|}{2} + \frac{1}{M} \left(\frac{Q}{2} - p_F \right) \right) \Psi = \left(\frac{E_{\pm}}{M} \right) \Psi,$$

$$\Psi(\mathbf{r}_{\perp} + 2\pi \mathbf{a}) = \exp \left(\frac{2\pi i (\mathbf{p}_{\perp} \cdot \mathbf{a})}{\alpha M_{\perp}} \right) \Psi(\mathbf{r}) \quad (17)$$

where $\mathbf{a} = (n, m)$ is a lattice vector. Remember that $Q/2 - p_F < 0$, so positive and negative branch conditions are not automatically satisfied. We have to choose appropriate regions for α and $|\mathbf{Q}|$.

Let us find such a region. The transverse equation can be solved analytically at small and large α . At $\alpha < 1$, we can approximate the potential as a sum of harmonic wells. For the negative branch,

$$\frac{E_-}{M} = \frac{1}{M} \left(\frac{Q}{2} - p_F \right) - 2 + 2\alpha - \frac{\alpha^2}{4} + O(\alpha^3)$$

$$- \frac{1}{2} \left(\cos \left(\frac{2\pi p_x}{\alpha M_{\perp}} \right) + \cos \left(\frac{2\pi p_y}{\alpha M_{\perp}} \right) \right) \exp \left(-\frac{\pi^2}{2\alpha} \right) \quad (18)$$

Since $(Q/2 - p_F) \sim -M$, the last term is small. At small α , $E_0 \approx -3 + O(\alpha)$, and satisfies the negative branch condition.

At large $\alpha \gg 1$, the spectrum E_- is dominated by the kinetic energy, $E_- \sim \alpha^2$, and is positive. Thus the spectrum crosses at some positive value of $\alpha \sim 1$, in agreement with the rough estimates of Eq. (8). When α reaches the critical value, the gap between the bands shrinks to zero at some point in the Brillouin zone, creating conditions for the emergence of new QCS with a wave vector at this point.

V. EFFECTIVE ACTION FOR THE COLLECTIVE EXCITATIONS.

We now derive the effective action for collective excitations. This is possible to do even without detailed knowledge of the quark correlation functions. We begin with the collective modes located on a particular patch, treating the curvature of the Fermi surface as a perturbation.

Consider two opposite patches of the Fermi surface connected by vector \mathbf{Q} , taking the z -axis along \mathbf{Q} . Diagonalizing the Dirac Hamiltonian for quarks close to the Fermi surface,

$$H_0 = \int dz d^2 \mathbf{x}_\perp \left\{ i(-R^\dagger \partial_z R + L^\dagger \partial_z L) + \frac{1}{2p_F} (\nabla_\perp R^\dagger \nabla_\perp R + \nabla_\perp L^\dagger \nabla_\perp L) + \dots \right\}; \quad (19)$$

where R, L fields represent right-moving and left-moving particles along z -direction. We suppress all indices, including those for spin. We consider N_f flavors in $3 + 1$ dimensions, so that fermion fields in one-dimensional chain effectively have $N'_f = 2N_f$ flavor indices.

We treat the system as many one-dimensional chains which couple through transverse kinetic terms. We discretize the transverse dimensions, so that the transverse degrees of freedom emerge as a result of interchain tunneling [16],

$$H_0 = \sum_{\mathbf{r}} \int dz \left\{ i(-R^\dagger(\mathbf{r}) \partial_z R(\mathbf{r}) + L^\dagger(\mathbf{r}) \partial_z L(\mathbf{r})) - t \sum_{\mathbf{a}} \left[R^\dagger(\mathbf{r}) R(\mathbf{r} + \mathbf{a}) + L^\dagger(\mathbf{r}) L(\mathbf{r} + \mathbf{a}) \right] \right\}. \quad (20)$$

Here \mathbf{a} are vectors connecting nearest neighbors, and t and a are chosen so that the spectrum of the discrete model approximates the continuous theory. The requirement of nearest neighbor tunneling is not necessary, and can be generalized, if need be. Choosing a square lattice, the resulting dispersion relation is

$$\epsilon_\perp(\mathbf{p}_\perp) = -2t \sum_{\mathbf{a}} \cos[\mathbf{a} \cdot \mathbf{p}_\perp] = -2t[\cos(p_x a) + \cos(p_y a) - 2] \quad (21)$$

In the continuum limit this dispersion relation reproduces $\mathbf{p}_\perp^2/2p_F$ on the interval set by (8):

$$ta^2 = 1/2p_F, \quad 8t = M. \quad (22)$$

Therefore $a^{-1} = (p_F M)^{1/2}/2 \sim M_\perp$. As we have shown in the previous subsection, the transverse dispersion can be substantially renormalized by the interaction between the patches, Eq. (18).

The Hamiltonian for each patch is ($\Phi = R + L$)

$$H = \sum_{\mathbf{r}} H_{1D}(\mathbf{r}) + T_{tunn} \quad (23)$$

$$H_{1D} = \int dz \left\{ i \left(-R^\dagger(\mathbf{r}) \partial_z R(\mathbf{r}) + L^\dagger(\mathbf{r}) \partial_z L(\mathbf{r}) \right) + \int dw \frac{g_{2D}^2}{2} (\Phi^\dagger t_A \Phi(\mathbf{r}, z)) |z - w| (\Phi^\dagger t_A \Phi(\mathbf{r}, w)) \right\} \quad (24)$$

$$T_{tunn} = -t \sum_{\mathbf{r}, \mathbf{a}} \left[R^\dagger(\mathbf{r}) R(\mathbf{r} + \mathbf{a}) + L^\dagger(\mathbf{r}) L(\mathbf{r} + \mathbf{a}) \right] \quad (25)$$

It is important that the interaction is essentially one-dimensional and is concentrated inside of each chain. One-dimensional models (24) can be treated by non-Abelian bosonization, as was done in [10]. The long range current-current interaction generates a gap of magnitude M in the color channel. The remaining gapless modes are described by the $U_{N_f' N_c}(1)$ and $SU_{N_c}(N_f')$ Wess-Zumino-Novikov-Witten (WZNW) models.

Some care must be taken in the normalization of quark fields, originally in $3 + 1$ dimensions, when we apply bosonization rules to the corresponding fields in $1 + 1$ dimensions. A one dimensional chain has resolution $\sim a^{-1} \sim M_\perp$ in the transverse direction, so it is necessary to multiply dimensionless fields by a^{-2} when we include the transverse dimensions, $z \rightarrow (z, \mathbf{r})$. For instance,

$$\bar{\Phi} \Phi(z, \mathbf{r}) \rightarrow a^{-2} \times C_{1D} (U \text{tr}[g] \text{tr}[h] + (h.c.)) \quad (26)$$

where the matrix valued fields U , g , and h on the right hand side are boson fields for $U(1)$, flavor, color sector. All of these fields are dimensionless. From the analysis of QCD in $1 + 1$ dimensions, C_{1D} has dimensions of mass, $\sim \Lambda_{\text{QCD}}$.

Next we treat Eq. (25) as a perturbation on the WZNW models. Turning on the transverse interactions, two things happen. While the single particle gap closes at the border of each patch, as discussed in the previous section, the gap is restored when we take into

account the fact that several patches meet at that point. In the mean field approximation, the size of the patch is given by Eq. (8). A more rigorous approach would be to use the exact 1D quark's Green's function for 1+1 dimensional QCD, and to use the Random Phase approximation (RPA) expression for the single quark Green's function, in the spirit of Ref. [16]:

$$G_{RR} = [G_{RR,1D}^{-1}(\omega, p_z) - \epsilon(\mathbf{p}_\perp)]^{-1}, \quad (27)$$

where $G_{RR,1D}$ is the Green's function for right-moving quarks in the one dimensional Hamiltonian of Eq.(24). A similar expression, with R replaced by L , holds for the left-moving quarks. Then the size of the patch is determined by the transverse momentum at which the Green's function (27) acquires a singularity at $\omega = 0$:

$$\frac{p_\perp^2}{2p_F} = \min G_{RR,1D}^{-1}(0, p_z) \quad (28)$$

At present we do not know the form of G_{1D} ; if we assume that

$$G_{1D}(0, p_z) = \frac{1}{p_z} f\left(\frac{p_z^2}{M^2}\right) \quad (29)$$

then we find that

$$\frac{(p_\perp^{\max})^2}{2p_F} = \beta M, \quad \beta \sim 1. \quad (30)$$

This agrees with the mean field estimate of Eq. (8).

The second effect of the interchain tunneling is that it generates a coupling between collective modes inside of a given patch. This occurs through virtual scattering processes, into states above the single particle gap. In the interaction picture for H_{1D} , time ordered product in second order in t generates the interchain coupling,

$$\begin{aligned} & t^2 \sum_{\mathbf{r}, \mathbf{r}', \mathbf{a}, \mathbf{a}'} \int d^2z d^2w [R^\dagger(z, \mathbf{r})R(z, \mathbf{r} + \mathbf{a})] [L^\dagger(w, \mathbf{r}' + \mathbf{a}')L(w, \mathbf{r}')] \\ & = -t^2 a^2 \sum_{\mathbf{r}, \mathbf{a}} \int d^2z d^2w [R_{fc}^\dagger(z, \mathbf{r})L_{f'c'}(w, \mathbf{r})] [L_{f'c'}^\dagger(w, \mathbf{r} + \mathbf{a})R_{fc}(z, \mathbf{r} + \mathbf{a})] + \dots, \end{aligned} \quad (31)$$

where f, c express flavor and color indices, respectively. We neglect terms where $\mathbf{r} \neq \mathbf{r}'$ or $\mathbf{a} \neq \mathbf{a}'$, which do not contribute at this order.

We integrate over the color sector, leaving color singlet operators. We use coherent field expressions, $L = (a^{-1}C_{1D}^{1/2}) \xi_L \xi_{Lf} \xi_{Lc}$ and $R = (a^{-1}C_{1D}^{1/2}) \xi_R \xi_{Rf} \xi_{Rc}$, which satisfy $\xi_R^\dagger \xi_L = U$,

$\xi_{Rf}^\dagger \xi_{Lf'} = g_{ff'}$, and $\xi_{Rc}^\dagger \xi_{Lc'} = h_{cc'}$. Due to $U(1)$ -flavor-color separation in H_{1D} , we can evaluate each sector separately. Note that only color sector has the scale $\sim \Lambda_{\text{QCD}} \sim M$. Further, correlation functions in the color sector damp rapidly, while those for the $U(1)$ and flavor sectors have power law correlations. This scale hierarchy allows us to use the following approximation:

$$\begin{aligned} \langle R_{fc}^\dagger(z) L_{f'c'}(w) \rangle_{H_{1D}}^{color} &= \frac{C_{1D}}{a^2} (\xi_R^\dagger(z) \xi_L(w)) (\xi_{Rf}^\dagger(z) \xi_{Lf'}(w)) \langle \xi_{Rc}^\dagger(z) \xi_{Lc'}(w) \rangle_{H_{1D}} \\ &\simeq \frac{C_{1D}}{a^2} (\xi_R^\dagger(z) \xi_L(z)) (\xi_{Rf}^\dagger(z) \xi_{Lf'}(z)) D_{cc'}(z-w) \\ &\simeq \frac{C_{1D}}{a^2} \Delta_{ff'}(z) (\delta_{cc'} g(z-w) + (t_A)_{cc'} f_A(z-w)), \end{aligned} \quad (32)$$

where $\Delta_{ff'} =: e^{i\Phi} :: g_{ff'} ::$. Therefore Eq.(31) becomes

$$\frac{\gamma N_c}{M^2} \times \left(-\frac{t^2 C_{1D}^2}{a^2} \right) \sum_{\mathbf{r}, \mathbf{a}} \int d^2 z \Delta_{ff'}(\mathbf{r}, z) \Delta_{f'f}^\dagger(\mathbf{r} + \mathbf{a}, z) + O(N_c^0). \quad (33)$$

The first factor arises from integration of correlation functions in color sector, and $\gamma \sim 1$. We have used the fact that correlation functions in the color sector contribute to integrals only within a distance $\sim M^{-1}$. Corrections $O(N_c^0)$ arise from color non-singlet operators.

We now have the effective Lagrangian for interchain coupling:

$$L_\perp = \frac{\gamma N_c C_{1D}^2}{(8a)^2} \sum_{\mathbf{r}, \mathbf{a}} \int d^2 z \text{tr}[\Delta(\mathbf{r}, z) \Delta^\dagger(\mathbf{r} + \mathbf{a}, z)] = \frac{\gamma N_c C_{1D}^2}{64} \int d^4 x \text{tr}[\partial_\perp \Delta(x) \partial_\perp \Delta^\dagger(x)] \quad (34)$$

where we used $8t = M$. For the unperturbed Hamiltonian, the correlation function of Δ scales as

$$\langle \Delta(\tau, z) \Delta(0, 0) \rangle_{H_{1D}} = \left[\frac{M^{-2}}{\tau^2 + z^2} \right]^{-d_\Delta}. \quad (35)$$

Here M serves as the ultraviolet cut-off. The scaling dimensions of the primary fields in the WZNW model are [17]:

$$d_\Delta = \left[\frac{1}{N_c N_f'} + \frac{N_f' - 1/N_f'}{N_c + N_f'} \right]. \quad (36)$$

Therefore the scaling dimension of the operator in Eq. (34) is less than two: that is, transverse hopping has generated relevant operators.

Near zero temperature, the system exhibits long range correlations. The massless modes inside of each patch couple strongly to one another, with an energy which depends on

their transverse momenta. Their three dimensional dynamics are described by the effective Lagrangian

$$\begin{aligned}\mathcal{L}_{k=N_c N'_f}^{U(1)} &= \frac{N'_f N_c p_F M}{8} \left[(\partial_L \Phi)^2 + \frac{\eta M}{p_F} (\partial_\perp \Phi)^2 \right], \\ \mathcal{L}_{k=N_c}^{SU(N'_f)} &= \frac{N_c p_F M}{4} \left[\mathcal{L}_{WZW}[g] + \frac{\eta' M}{p_F} \text{tr}[\partial_\perp g \partial_\perp g^\dagger] \right],\end{aligned}\quad (37)$$

where

$$\mathcal{L}_{WZW}[g] = \frac{1}{16\pi} \text{tr}[\partial_L g \partial_L g^\dagger] + i \frac{\epsilon_{\mu\nu\lambda}}{24\pi} \int d\xi \text{tr}[(g^\dagger \partial^\mu g)(g^\dagger \partial^\nu g)(g^\dagger \partial^\lambda g)]. \quad (38)$$

Here ∂_L express derivatives for time and longitudinal directions. We have omitted corrections $O(M^2/p_F^2, 1/N_c)$, with the constants $\eta, \eta' \sim 1$.

In one spatial dimension, due to infrared fluctuations there is only quasi long range order. After including transverse hopping, our gapless modes become three dimensional, Eq. (37), which drastically decreases the role of infrared fluctuations. Consequently, in three dimensions there is true long range order, and a well defined ground state. (In contrast to Ref. [18], this is only seen when transverse fluctuations are included.)

Another consequence of the increase in the spatial dimensionality is that nonlinear terms in the WZNW action can be treated perturbatively. Goldstone modes of a QCS have a spectrum

$$\omega_{\mathbf{n}}^2(\mathbf{p}) = (\mathbf{n} \cdot \mathbf{p})^2 + \kappa \left(\frac{M}{p_F} \right) [\mathbf{n} \times \mathbf{p}]^2, \quad \kappa \sim \eta, \eta'. \quad (39)$$

The unit vector \mathbf{n} is the wave vector of the QCS, with momenta measured from north or south pole of the Fermi surface, $p_F \mathbf{n}$. This expression is valid for $|\mathbf{p}_\perp| \ll M_\perp$. It is not valid close to the boundary of a patch, where one cannot expand in t , and effects from other patches must be included. This shows that at high density the spectrum is less sensitive to the transverse momenta, in accord with Ref. [10].

Finally we mention interactions among quantum excitations. Since Eq.(37) has a decay constant of $O(N_c)$, higher order couplings of quantum excitations always accompany suppression factor of $O(1/N_c)$, in a similar way as chiral Lagrangian. Therefore, in large N_c , dynamics close to the Fermi surface is described by free Goldstone bosons. The interaction between coherent excitations are interesting and will be discussed elsewhere.

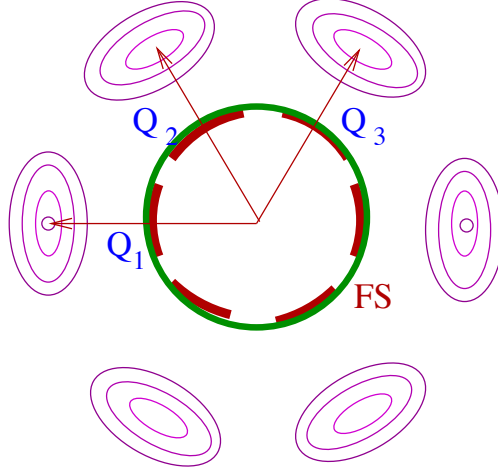


FIG. 3: The schematic picture of collective excitations for the Fermi surface with three QCSs. The magenta ellipses of various intensity correspond to surfaces of constant $\omega(\mathbf{p})$. The dark areas represent regions of momentum space where the Goldstone modes are subject to decay into quarks. The green circle is the original FS. The red arcs represent the portions of FS where spectral gaps emerge.

VI. CONCLUSIONS

In a Quarkyonic regime, where quarks are confined, instead of treating the entire Fermi surface, it is more natural to first construct mesonic degrees of freedom within a particular momentum region. Since gaps arise from confinement, the gap energy is almost independent of density.

We analyzed multiple patches of QCSs based on results for a single patch. In going from one to multiple patches, it is essential to remember that interactions between particles (or holes) and QCSs are suppressed at large angles. Then each patch can be treated incoherently, except at boundaries where several patches meet. Knowing the magnitude of the gap allowed us to estimate the size of each patch.

We derived the effective Lagrangian for Goldstone modes by regarding the system as one dimensional chains with weak transverse tunnelings. After inclusion of transverse hopping effects, the spectrum of Goldstone bosons propagate in three dimensions. As a consequence, quasi-long range order in $1 + 1$ dimensions becomes, in $3 + 1$ dimensions, true long range order. Corrections can be systematically estimated through an expansion in Λ_{QCD}/p_F .

Our arguments imply that as the quark density increases, the Fermi surface acquires more patches, which have an increasingly large symmetry. Accordingly, there is a series of phase transitions as the symmetry of the Fermi surface increases. At the same time, the Goldstone bosons become more like those in $1 + 1$ dimensions. Then long range order in $3 + 1$ dimensions becomes closer to quasi-long range order in $1 + 1$ dimensions. This suggests that both chiral and rotational symmetries are effectively restored, but in a manner rather different from common assumption.

VII. ACKNOWLEDGMENTS

We are grateful to Y. Hidaka, L. McLerran, A. Rebhan, and A. Schmitt for discussions and interest in our work. The research of R. D. Pisarski and A. Tsvetik are supported under the US Department of Energy Contract No. DE-AC02-98CH10886. T. Kojo is supported by the Special Postdoctoral Research Program of RIKEN. R. D. Pisarski also thanks the Alexander von Humboldt Foundation for their support.

-
- [1] M. G. Alford, A. Schmitt, K. Rajagopal and T. Schafer, *Rev. Mod. Phys.* **80**, 1455 (2008) [[arXiv:0709.4635](#)], and references therein.
 - [2] D. V. Deryagin, D. Y. Grigoriev and V. A. Rubakov, *Intl. Jour. Mod. Phys. A* **7**, 659 (1992).
 - [3] E. Shuster and D. T. Son, *Nucl. Phys. B* **573**, 434 (2000) [[arXiv:hep-ph/9905448](#)].
 - [4] B. Y. Park, M. Rho, A. Wirzba and I. Zahed, *Phys. Rev. D* **62**, 034015 (2000) [[arXiv:hep-ph/9910347](#)]; R. Rapp, E. V. Shuryak and I. Zahed, *ibid.* **63**, 034008 (2001); [[arXiv:hep-ph/0008207](#)].
 - [5] B. Bringoltz, *Jour. High Energy Phys.* **0703**, 016 (2007); [[arXiv:hep-lat/0612010](#)]. *Phys. Rev. D* **79**, 105021 (2009) [[arXiv:0811.4141](#)]; *ibid.* **79**, 125006 (2009) [[arXiv:0901.4035](#)].
 - [6] L. McLerran and R. D. Pisarski, *Nucl. Phys. A* **796**, 83 (2007) [[arXiv:0706.2191](#)].
 - [7] Y. Hidaka, L. D. McLerran and R. D. Pisarski, *Nucl. Phys. A* **808**, 117 (2008) [[arXiv:0803.0279](#)].
 - [8] K. Fukushima, *Phys. Rev. D* **77**, 114028 (2008) [Erratum-*ibid.* *D* **78**, 039902 (2008)]. [[arXiv:0803.3318](#)].

- [9] A. Andronic *et al.*, [[arXiv:0911.4806](#)].
- [10] T. Kojo, Y. Hidaka, L. McLerran and R. D. Pisarski, [[arXiv:0912.3800](#)].
- [11] L. Y. Glozman and R. F. Wagenbrunn, Phys. Rev. D **77**, 054027 (2008) [[arXiv:0709.3080](#)];
L. Y. Glozman, *ibid.* **79**, 037504 (2009) [[arXiv:0812.1101](#)]; *ibid.* **80**, 037701 (2009)
[[arXiv:0907.1473](#)].
- [12] P. Guo and A. P. Szczepaniak, Phys. Rev. D **79**, 116006 (2009) [[arXiv:0902.1316](#)].
- [13] V. Schon and M. Thies, Phys. Rev. D **62**, 096002 (2000); M. Thies, *ibid.* **69**, 067703 (2004);
M. Thies and K. Urlichs, *ibid.* **67**, 125015 (2003); *ibid.* **71**, 105008 (2005); *ibid.* **72**, 105008
(2005); O. Schnetz, M. Thies and K. Urlichs, Annals Phys. **321**, 2604 (2006); C. Boehmer,
M. Thies and K. Urlichs, Phys. Rev. D **75**, 105017 (2007). G. Basar and G. V. Dunne, Phys.
Rev. Lett. **100**, 200404 (2008); Phys. Rev. D **78**, 065022 (2008); C. Boehmer, U. Fritsch,
S. Kraus and M. Thies, *ibid.* **78**, 065043 (2008); G. Basar, G. V. Dunne and M. Thies, *ibid.*
79, 105012 (2009); C. Boehmer and M. Thies, [[arXiv:0912.2664](#)].
- [14] A. Tsvetik, *Quantum Field Theory in Condensed Matter Physics* (Cambridge University Press,
Cambridge, 2003).
- [15] G. 't Hooft, Nucl. Phys. B **75**, 461 (1974).
- [16] F. H. L. Essler and A. M. Tsvetik, Phys. Rev. B **65**, 115117 (2002); Phys. Rev. B **71**, 195116
(2005).
- [17] V. G. Knizhnik and A. B. Zamolodchikov, Nucl. Phys. B **247**, 83 (1984).
- [18] G. Baym, B. L. Friman and G. Grinstein, Nucl. Phys. B **210**, 193 (1982).